Computation of fast depressurization of water using a two-fluid model: revisiting Bilicki modelling of mass transfer

Hippolyte Lochon, Frédéric Daude, Pascal Galon, Jean-Marc Hérard

Computation of fast depressurization of water using a two-fluid model: revisiting Bilicki modelling of mass transfer

H. Lochon[a,b,e], F. Daude[a,b], P. Galon[b,c], and J.-M. Hérard[d,e]

[a]EDF R&D, Département AMA, 7 Boulevard Gaspard Monge, 91120 Palaiseau, France
[b]IMSIA, UMR EDF/CNRS/CEA/ENSTA 9219, Université Paris-Saclay, 828 Boulevard des Maréchaux, 91762 Palaiseau Cedex, France
[c]CEA, DEN, DANS, DM2S, SEMT, DYN, 91191 Gif-sur-Yvette Cedex, France
[d]EDF R&D, Département MFEE, 6 Quai Watier, 78401 Chatou Cedex, France
[e]I2M, UMR CNRS 7373, Technopôle Château-Gombert, 39 rue F. Joliot Curie, 13453 Marseille Cedex 13, France

Abstract

This paper is devoted to the computation of the fast depressurization of water using a two-fluid model. Such application, which is extensively studied in the nuclear field, involves many interactions between two phenomena, the mass transfer and the propagation of pressure waves. A simple but physically-based modelling of the mass transfer for the depressurization of water is proposed, which relies on the work of Bilicki & Kestin [4] in the homogeneous frame. Four different experiments have been chosen to assess the proposed model. Three of them study the depressurisation of hot water in a pressurized pipe. The comparison between converged numerical results and the experimental data shows a good agreement and demonstrates the ability of the two-fluid-model to capture the proper mass transfer for a wide range of thermodynamical conditions. The last test-case is the HDR experiment which considers the depressurization of a full-scale vessel under the hypothesis of a Loss Of Coolant Accident. The results of an ALE computation show the ability of the proposed model to retrieve experimental data in both structure and fluid.

1 Introduction

Compressible two-phase flows are involved in many industrial applications such as naval engineering, petroleum industry, nuclear power generation, automative or aerospace technologies. In the nuclear field, two-phase flows are mainly steam-water flows in Pressurized Water Reactors (PWR). Since the 1960s, many two-phase flow models have been proposed for nuclear thermal hydraulics. Most of the modelling efforts have been made to predict the Loss-Of-Coolant-Accident (LOCA) which is one of the basic failure mode of PWR. In such transient steam-water flows, two main physical phenomena are involved and highly interact with each other, the propagation of pressure waves and the mass transfer. The interactions with the structure surrounding the fluid should also be taken into account when the amplitudes of pressure waves are strong.

Two different approaches are usely distinguished to model two-phase flows: the homogeneous approach and the two-fluid approach. Models based on the first approach consider the mixture of the two phases as one fluid assuming different equilibria between both phases. In the second approach, no phasic equilibrium is assumed and two different fluids are considered. As a consequence, many transfers between the two phases, including the mass transfer, require proper modelling. Ransom and Hicks [33] proposed one of the first models based on this second approach. Since then, the two-fluid approach has gained interest and many models can be found in the literature, see [3, 25, 20, 36, 18, 16] among others.

The present work is dedicated to the modelling of the fast depressurization of water following the two-fluid approach. Thus, the governing equations of the model are obtained using a classical

statistical averaging of the local conservation laws [23, 11]. The corresponding model is hyperbolic but cannot be written in a fully conservative form. It also requires closure laws for interfacial quantities involved in the non-conservative terms and for the source terms. Based on the comparison of different two-fluid models on steam-water transients proposed in [29], the closure laws of the Baer-Nunziato model [3] have been chosen for the interfacial pressure and velocity. As in previous work [22, 7], the modelling of the source terms is based on relaxation phenomena to comply with the entropy inequality. Thus, several relaxation time scales are involved in the transfers between phases and require proper modelling. Evaluations of the pressure and velocity relaxation time scales can be found in [29] whereas the chemical potential relaxation, which corresponds to the mass transfer, requires further work. In order to propose simple but physically-based evaluation of this time scale, we focus on the work of Bilicki and co-authors [4, 5, 10] on the Homogeneous Relaxation Model. Based on the same approach, a simple evaluation of the temperature relaxation time scale is also proposed. As in [7], particular attention is paid to the validation of the proposed model. Four different experiments studying the fast depresussurisazion of water have been chosen to that end.

Hence the paper is organized as follows. We first present the governing equations of the two-fluid model with the complete sets of closure laws including the non-conservative terms and the source terms. The main mathematical properties of the model are briefly recalled. Then, the evaluation of the four relaxation time scales involved in the source terms are discussed. The modelling of the mass transfer in the current model is compared, under some hypothesis, to the one proposed by Bilicki *et al.* [4] in the Homogeneous Relaxation Model. Thus, an evaluation of the chemical potential relaxation time scale is obtained. The second section of the paper is dedicated to the validation of the proposed model with the Bilicki-like mass transfer. The numerical methods used for the computation of the two-fluid model are briefly presented with associated references. Four experiments have been chosen to assess the proposed model. Three of them study the fast depressurization of hot water from a pressurized pipe: the Canon, Super-Canon and Edwards pipe experiments. 1D converged numerical results of the two-fluid model with and without the Bilicki-like mass transfer model are compared to the experimental data. The comparison shows that the proposed Bilicki-like mass transfer significantly improves the results of the two-fluid model for a wide range of thermodynamical states. The last test-case is the HDR experiment which studies the depressurization of a full-scale vessel under the hypothesis of a LOCA. Both pressures in the fluid and diplacements of internal structures are measured in the vessel during the experiment allowing to focus on the mechanical consequences of a LOCA. A 3D Arbitrary Lagrangian-Eulerian computation taking into account the Fluid-Structure Interactions is carried out and numerical results show a fair agreement with experimental measurements in both structure and fluid.

2 The two-fluid model

The derivation of two-fluid models is based on classical statistical averaging of local conservation laws [23, 11]. Relevant closure laws are required in the construction and the entropy inequality is a major tool to derive them [18, 16, 24, 31].

2.1 Governing equations

The two-fluid model considered here that does not assume any equilibrium between the two phases. Throughout the paper, the subscript k refers to the phase ($k = v$ for the vapor and $k = l$ for the liquid). $\alpha_k \in]0, 1[$ is the statistical fraction of phase k and complies with the following relation:

$$\alpha_v + \alpha_l = 1$$

We denote ρ_k the mean density of phase k, u_k its mean velocity, p_k its mean pressure and e_k its mean specific total energy complying with:

$$e_k = \varepsilon_k + \frac{1}{2}u_k^2 \tag{1}$$

ε_k is the mean specific internal energy of phase k which is linked to the mean density and pressure of phase k by an Equation Of State (EOS):

$$\varepsilon_k = \varepsilon_k\left(\rho_k, p_k\right) \tag{2}$$

Based on the EOS, the celerity c_k of acoustic waves as well as the specific entropy s_k of phase k can be defined. They comply with the following relations:

$$\rho_k c_k^2 = \left(\partial_{p_k}\varepsilon_k\right)^{-1}\left(\frac{p_k}{\rho_k} - \rho_k\left(\partial_{\rho_k}\varepsilon_k\right)\right) \tag{3}$$

$$c_k^2\left(\partial_{p_k} s_k\right) + \left(\partial_{\rho_k} s_k\right) = 0 \tag{4}$$

Thus, the governing equations of the two-fluid model read:

$$\left\{\begin{array}{lcll} \partial_t\left(\alpha_k\right) & + & u_I\ \partial_x\left(\alpha_k\right) & = S_{1,k} \\ \partial_t\left(\alpha_k\rho_k\right) & + & \partial_x\left(\alpha_k\rho_k u_k\right) & = S_{2,k} \\ \partial_t\left(\alpha_k\rho_k u_k\right) & + & \partial_x\left(\alpha_k\rho_k u_k^2 + \alpha_k p_k\right) - p_I\ \partial_x\left(\alpha_k\right) & = S_{3,k} \\ \partial_t\left(\alpha_k\rho_k e_k\right) & + & \partial_x\left(\alpha_k\rho_k e_k u_k + \alpha_k p_k u_k\right) - p_I u_I\ \partial_x\left(\alpha_k\right) & = S_{4,k} \end{array}\right. \tag{5}$$

Many closure laws for the interfacial velocity and pressure (u_I, p_I) have been proposed in the literature [3, 6, 19, 36] and some of them have been compared for steam-water transients in [29]. *In the sequel, we consider the closure laws proposed by Baer & Nunziato [3], given by the following:*

$$\left(u_I, p_I\right) = \left(u_l, p_v\right) \tag{6}$$

The closure laws for the source terms $S_{j,k}$ $(j = 1, 4)$ on the right-hand side are the following:

$$\begin{array}{lcl} S_{1,k} & = & \Phi_k \\ S_{2,k} & = & \Gamma_k \\ S_{3,k} & = & D_k + \mathcal{U}\Gamma_k \\ S_{4,k} & = & Q_k + \mathcal{U}D_k + \mathcal{H}\Gamma_k - p_I\Phi_k \end{array} \tag{7}$$

where $\mathcal{U} = \frac{1}{2}(u_v + u_l)$ and $\mathcal{H} = \frac{1}{2}(u_v u_l)$. The different contributions are written as relaxation phenomena:

$$\begin{array}{lcll} \Phi_k & = & \dfrac{1}{\tau_p p_{ref}}\alpha_k\alpha_j\left(p_k - p_j\right) & \\ \Gamma_k & = & \dfrac{1}{\tau_\mu \mu_{ref}}\dfrac{m_k m_j}{m_k + m_j}\left(\mu_j - \mu_k\right) & \\ D_k & = & \dfrac{1}{\tau_u}\dfrac{m_k m_j}{m_k + m_j}\left(u_j - u_k\right) & , \quad j \neq k \\ Q_k & = & \dfrac{1}{\tau_T}\dfrac{m_k C_{V\,k} m_j C_{V\,j}}{m_k C_{V\,k} + m_j C_{V\,j}}\left(T_j - T_k\right) & \end{array} \tag{8}$$

where $C_{V\,k}$ is the heat capacity at constant volume of phase k, $m_k = \alpha_k\rho_k$ and $\mu_k = \dfrac{g_k}{T_k}$. T_k is the temperature of phase k and g_k its specific Gibbs enthalpy:

$$\frac{1}{T_k} = \left(\partial_{p_k}\varepsilon_k\right)^{-1}\left(\partial_{p_k} s_k\right) \tag{9}$$

$$g_k = \varepsilon_k + \frac{p_k}{\rho_k} - T_k s_k \tag{10}$$

Each relaxation phenomenum involves a relaxation time scale τ_φ which drives the quantity φ ($\varphi = p, \mu, u, T$) towards the phasic equilibrium. Finally p_{ref} and μ_{ref} are respectively a reference pressure and a reference potential.

2.2 Main properties of the model

We may now recall the main properties of the two-fluid model (5) with the Baer-Nunziato closure law (6). The first property focuses on the entropy of the global model whereas the other properties deal with the convective part of the model which was first studied by Embid & Baer [13].

- **Entropy inequality**
  Smooth solutions of system (5) comply with an entropy inequality:

$$\begin{aligned}\partial_t\left(\sum_k m_k s_k\right)+\partial_x\left(\sum_k m_k s_k u_k\right) = \quad & (\mu_l-\mu_v)\,\Gamma_v \\ & +\frac{1}{T_l}\,(p_v-p_l)\,\Phi_v \\ & +\left(\frac{1}{2T_v}+\frac{1}{2T_l}\right)(u_l-u_v)\,D_v \\ & +\left(\frac{1}{T_v}-\frac{1}{T_l}\right)Q_v \qquad \geq 0 \end{aligned} \tag{11}$$

- **Hyperbolicity and structure of waves**
  The convective part of system (5):

$$\left\{\begin{array}{lcll} \partial_t(\alpha_k) & + & u_I\ \partial_x(\alpha_k) & = 0 \\ \partial_t(\alpha_k\rho_k) & + & \partial_x(\alpha_k\rho_k u_k) & = 0 \\ \partial_t(\alpha_k\rho_k u_k) & + & \partial_x\left(\alpha_k\rho_k u_k^2+\alpha_k p_k\right)-p_I\ \partial_x(\alpha_k) & = 0 \\ \partial_t(\alpha_k\rho_k e_k) & + & \partial_x(\alpha_k\rho_k e_k u_k+\alpha_k p_k u_k)-p_I u_I\ \partial_x(\alpha_k) & = 0 \end{array}\right. \tag{12}$$

  is hyperbolic. It admits six real eigenvalues:

$$\begin{array}{lllllll} \lambda_1 & = & u_v-c_v, & \lambda_2 & = & u_v, & \lambda_3 & = & u_v+c_v, \\ \lambda_4 & = & u_l-c_l, & \lambda_{5,6} & = & u_l, & \lambda_7 & = & u_l+c_l \end{array} \tag{13}$$

  and associated righteigenvectors span the whole space $\mathbb{R}^7$ if $|u_l-u_v|\neq c_v$. Fields associated with eigenvalues $\lambda_{2,5,6}$ are linearly degenerate (LD) whereas fields associated with eigenvalues $\lambda_{1,3,4,7}$ are genuinely non linear (GNL).

- **Jump conditions**
  Unique jump conditions hold within each isolated field. Moreover, classical single phase jump relations hold in the GNL fields:

$$\left\{\begin{array}{l} [\alpha_k]=0 \\ -\sigma[\rho_k]+[\rho_k u_k]=0 \\ -\sigma[\rho_k u_k]+\left[\rho_k u_k^2+p_k\right]=0 \\ -\sigma[\rho_k e_k]+[\rho_k e_k u_k+p_k u_k]=0 \end{array}\right. \tag{14}$$

  where $[\varphi]=\varphi_R-\varphi_L$ is the jump between the Left and Right states on each side of a shock wave traveling at speed σ.

The three properties are crucial from both theoretical and numerical points of view. We underline the fact that the 5,6-field is LD ; thus the non-conservative products of the model are properly defined and not active in GNL fields. More details on those properties could be found in [6, 16, 21].

2.3 Evaluation of relaxation time scales

This section is dedicated to the evaluation of the four relaxation time scales τ_φ ($\varphi = p, \mu, u, T$) in the case of the fast depressurization of water. Such an evaluation is difficult to provide and most available work in the literature deals with instantaneous relaxation [27, 32, 9]. Since the underlying physical phenomena are far from being instantaneous in many applications, we only consider non-instantaneous relaxations in the present work. For pressure and velocity relaxations, we consider the time scales used in [29] for steam-water transients. The chemical potential relaxation corresponds to the mass transfer Γ_k and a new evaluation of its time scale is proposed based on the work of Bilicki *et al.* [4, 10]. Finally, we propose a simple evaluation of the temperature relaxation time scale.

2.3.1 Pressure relaxation

Based on [17], the pressure relaxation time scale is evaluated using the Rayleigh-Plesset equation, which considers the evolution of a bubble in an infinite medium. It provides the following evaluation:

$$\tau_p p_{ref} = \begin{cases} \frac{4}{3}\eta_l & \text{if } \alpha_v < \alpha_{min} \\ \frac{4}{3}\eta_v & \text{if } \alpha_v > \alpha_{max} \\ \left(\frac{\alpha_{max}-\alpha_v}{\alpha_{max}-\alpha_{min}}\right)\frac{4}{3}\eta_l + \left(\frac{\alpha_v-\alpha_{min}}{\alpha_{max}-\alpha_{min}}\right)\frac{4}{3}\eta_v & \text{otherwise} \end{cases} \tag{15}$$

where η_k is the dynamic viscosity of phase k.

2.3.2 Velocity relaxation

The behavior of a bubble in an infinite medium is also considered for the velocity relaxation. Thus the evaluation of the corresponding time scale is based on the drag equation. More precisely, we consider the following model proposed in the NEPTUNE-CFD code [26] for liquid-gas separated flows:

$$D_k = \alpha_k \alpha_j F_D(\alpha_v)\,(u_j - u_k) \quad , \quad j \neq k \tag{16}$$

where the function F_D of α_v is defined as follows:

$$F_D(\alpha_v) = \begin{cases} F_{D,v}(1-\alpha_v) & \text{if } \alpha_v < \alpha_{min} \\ F_{D,l}(\alpha_v) & \text{if } \alpha_v > \alpha_{max} \\ \left(\frac{\alpha_{max}-\alpha_v}{\alpha_{max}-\alpha_{min}}\right)F_{D,v}(1-\alpha_{min}) + \left(\frac{\alpha_v-\alpha_{min}}{\alpha_{max}-\alpha_{min}}\right)F_{D,l}(\alpha_{max}) & \text{otherwise} \end{cases}$$

The function F_D is equal to the function $F_{D,p}(\alpha_q)$ in the case of isolated spherical inclusions of phase p in the continuous phase q. The following classic correlations are used [1, 26]:

$$F_{D,p}(\alpha_q) = \frac{3}{4}\frac{\rho_q}{\alpha_q}\frac{C_{D,p}}{d_p}\,|u_p - u_q| \qquad , \qquad q \neq p$$

with:

$$C_{D,p} = \frac{24}{Re_p}\left(1 + 0.15\,(Re_p)^{0.687}\right) \quad \text{and} \quad Re_p = \frac{\rho_q d_p}{\eta_q}\,|u_p - u_q|$$

where d_p is a characteristic diameter of the inclusion. It is defined using the critical Weber number $We = 10$ (see [1]) and the surface tension σ of the liquid phase:

$$We = \frac{\rho_q d_p}{\sigma}\,|u_p - u_q|^2$$

Thus, the evaluation of the velocity relaxation time scale is obtained using (8) and (16):

$$\tau_u = \frac{\rho_v \rho_v}{m_v + m_l} \frac{1}{F_D(\alpha_v)} \tag{17}$$

2.3.3 Chemical potential relaxation

The chemical potential relaxation corresponds to the mass transfer Γ_k. Therefore we focus on the modelling of the mass transfer used by Bilicki *et al.* [4, 10] for the depressurization of water in order to propose an evaluation of the chemical potential relaxation time scale. The Homogeneous Relaxation Model (HRM) of Bilicki & Kestin [4] is detailed in 4. Downar-Zapolski *et al.* [10] proposed a correlation for the relaxation time scale involved in this model based on the results of the Moby Dick experiments [34]. Although this correlation has been determined in the stationary case, it has been used in the transient case with both homogeneous [14] and two-fluid [15] models.

In order to propose an evaluation of the time scale τ_μ based on the model proposed by Bilicki & Kestin [4] in the homogeneous frame, we assume that that both phases are in an homogeneous state ($\partial_x(\varphi) = 0, \forall \varphi$) at rest ($u_k = 0$) with the following thermodynamical equilibrium: $p_v = p_l$ and $T_v = T_l$. Based on those hypothesis, the governing equations of the two-fluid model (5) become:

$$\left\{ \begin{array}{lcl} \partial_t(\alpha_k) & = & 0 \\ \partial_t(\alpha_k \rho_k) & = & \Gamma_k \\ \partial_t(\alpha_k \rho_k u_k) & = & 0 \\ \partial_t(\alpha_k \rho_k e_k) & = & 0 \end{array} \right. \tag{18}$$

We can recast this system in the following way:

$$\left\{ \begin{array}{lcl} \partial_t(\alpha_k) & = & 0 \\ \partial_t(m_k) & = & \Gamma_k \\ \partial_t(m_k u_k) & = & 0 \\ \partial_t(m_k \varepsilon_k) & = & 0 \end{array} \right. \tag{19}$$

Thus, the thermodynamical variable μ_k, whose desequilibrium drives the mass transfer Γ_k, can be written as a function of the partial mass m_k only. Indeed:

$$\mu_k = \mu_k(\rho_k, \varepsilon_k) = \mu_k\left(\frac{m_k}{\alpha_k^0}, \frac{m_k^0 \varepsilon_k^0}{m_k}\right)$$

where we use the notation $\varphi^0 = \varphi(t=0)$. To provide a deeper analysis of the mass transfer, we assume that both phases are governed by the Stiffened Gas EOS:

$$\left\{ \begin{array}{lcl} \varepsilon_k & = & \left((\gamma_k - 1)\rho_k\right)^{-1}\left(p_k + \gamma_k p_k^\infty\right) \; + \; q_k \\ T_k & = & \left(C_{Vk}(\gamma_k - 1)\rho_k\right)^{-1}\left(p_k + p_k^\infty\right) \\ s_k & = & C_{Vk} \ln\left(\left(C_{Vk}\left(\gamma_k - 1\right)\rho_k\right)^{-\gamma_k}\left(p_k + p_k^\infty\right)\right) \; + \; q_k' \end{array} \right. \tag{20}$$

We also assume that $q_k = 0$. Based on this particular choice of the EOS, the function $\mu_k(m_k)$ can be expressed in the following way:

$$\mu_k(m_k) = C_{Pk} + C_{Pk} \ln(m_k) - \mathcal{S}_k^0 \tag{21}$$

where we use the following constants :

$$C_{Pk} = \gamma_k C_{Vk} \quad \text{and} \quad \mathcal{S}_k^0 = C_{Vk} \ln\left(\frac{\left(p_k^0 + p_k^\infty\right)\left(\alpha_k^0\right)^{\gamma_k}}{\left(C_{Vk}\left(\gamma_k - 1\right)\right)^{\gamma_k}}\right) + q_k'$$

Let us now focus on the difference $\mu_j - \mu_k$. An important remark is that those quantities are equal at the thermodynamical and chemical equilibrium since both temperatures and chemical potentials would be equal: $\overline{\mu_j} = \overline{\mu_k}$. Therefore, this difference could be written in the following way:

$$\begin{aligned}
\mu_j - \mu_k &= \left(\mu_j - \overline{\mu_j}\right) - \left(\mu_k - \overline{\mu_k}\right) \\
&= \left(\mu_j(m_j) - \mu_j(\overline{m_j})\right) - \left(\mu_k(m_k) - \mu_k(\overline{m_k})\right) \\
&= C_{Pj} \ln\left(\frac{m_j}{\overline{m_j}}\right) - C_{Pk} \ln\left(\frac{m_k}{\overline{m_k}}\right)
\end{aligned}$$

Finally, a last hypothesis is being made, we assume that the two-phase flow is close to the thermodynamical and chemical equilibrium: $m_k \approx \overline{m_k}$. Noticing that $m_k + m_j = \overline{m_k} + \overline{m_j}$, we get:

$$\begin{aligned}
\mu_j - \mu_k &= C_{Pj} \ln\left(\frac{m_j}{\overline{m_j}}\right) - C_{Pk} \ln\left(\frac{m_k}{\overline{m_k}}\right) \\
&\approx C_{Pj} \frac{m_j - \overline{m_j}}{\overline{m_j}} - C_{Pk} \frac{m_k - \overline{m_k}}{\overline{m_k}} \\
&\approx -\frac{C_{Pj}\overline{m_k} + C_{Pk}\overline{m_j}}{\overline{m_j}\ \overline{m_k}} \left(m_k - \overline{m_k}\right)
\end{aligned}$$

Thus, we obtain the following approximation of the mass transfer, defined in equation (8):

$$\Gamma_k \approx -\frac{1}{\tau_\mu \mu_{ref}} \frac{C_{Pj}\overline{m_k} + C_{Pk}\overline{m_j}}{\overline{m_k} + \overline{m_j}} \left(m_k - \overline{m_k}\right) \quad , \quad j \neq k \tag{22}$$

If we compare it to the closure law proposed by Bilicki and Kestin [4] and given in equation (32), we have:

$$\tau_\mu \mu_{ref} \approx \frac{C_{Pj}\overline{m_k} + C_{Pk}\overline{m_j}}{\overline{m_k} + \overline{m_j}}\ \theta \tag{23}$$

Therefore, we propose the following evaluation of the time scale τ_μ and the reference potential μ_{ref}:

$$\tau_\mu = \theta \qquad \text{and} \qquad \mu_{ref} = \begin{cases} C_{Pv} & \text{if } \alpha_v < \alpha_{min} \\ C_{Pl} & \text{if } \alpha_v > \alpha_{max} \\ \left(\dfrac{\alpha_{max} - \alpha_v}{\alpha_{max} - \alpha_{min}}\right) C_{Pv} + \left(\dfrac{\alpha_v - \alpha_{min}}{\alpha_{max} - \alpha_{min}}\right) C_{Pl} & \text{otherwise} \end{cases} \tag{24}$$

where θ is defined as follows (see [10] and the recent study in [28]):

$$\theta \ = \ 6.51 \times 10^{-7}\ \alpha_v^{-0.257} \left(\frac{p_{sat} - p}{p_{sat}}\right)^{-2.24} \tag{25}$$

using the mean pressure $p = \alpha_v p_v + \alpha_l p_l$. *The use of this time scale will be referred to as Bilicki-like mass transfer in the sequel.*

2.3.4 Temperature relaxation

In order to propose a simple evaluation of the temperature relaxation time scale, we assume that this phenomenum is mainly driven by the vaporisation. This hypothesis is relevant for steam-water transients such as the depressurization of water since the heat diffusion can be neglected in those fast applications. Thus, we have the following evaluation of the time scale:

$$\tau_T \ = \ \tau_\mu \tag{26}$$

3 Numerical results

In order to assess the proposed modelling of the mass transfer, four different experiments have been selected. Three of them (the Canon experiment, the Super-Canon experiment [35] and the Edwards pipe experiment [12]) study the rapid depressurization of hot liquid water from an horizontal pipe with similar characteristics (a length of about 4 m and a constant inner diameter of about 10 cm). The pipe has a closed end at one side and a membrane on the other side. At time zero, the membrane is broken and a rarefaction wave starts propagating along the pipe. At the final time, water is fully turned into vapor therefore these are excellent test-cases to study the mass transfer. Those experiments are classical test cases for nuclear safety codes in order to study the Loss-Of-Coolant-Accident (LOCA). The main difference between the three experiments lies in the initial conditions, summarized in table 1. The last experiment, which has been carried out by the HDR (Heißdampfreaktor) Safety Program in Germany [37], studies the depressurization of a full-scale reactor vessel under the hypothesis of a LOCA. Many measurements of pressure and displacement in the vessel are provided so that mechanical consequences of the depressurization can be studied unlike the three other test-cases.

Table 1: Initial conditions of liquid water in the different experiments

Experiment	Pressure (Bar)	Temperature (°C)
Canon	32	220
Super-Canon	150	300
Edwards pipe	70	242

A fractionnal step method is used for the computation of the two-fluid model with source terms (system (5)). A key property of this method, proposed in [22] without mass transfer, is to be consistent with the entropy inequality of the model (equation (11)). It was then extended to the case with mass transfer in [7, 29]. We also use the first-order HLLC-type convective solver recently proposed in [30], with a Courant number $C_{CFL} = max(\lambda_k)\frac{\Delta t}{\Delta x} = 0.5$. The Equation Of State used in the computations is the Stiffened Gas EOS:

$$\left\{ \begin{array}{rcl} \varepsilon_k & = & \left((\gamma_k - 1)\rho_k\right)^{-1}\left(p_k + \gamma_k p_k^{\infty}\right) \ + \ q_k \\ T_k & = & \left(C_{V\,k}(\gamma_k - 1)\rho_k\right)^{-1}\left(p_k + p_k^{\infty}\right) \\ s_k & = & C_{V\,k}\ln\Big(\left(C_{V\,k}\left(\gamma_k - 1\right)\rho_k\right)^{-\gamma_k}\left(p_k + p_k^{\infty}\right)\Big) \ + \ q_k' \end{array} \right. \tag{27}$$

Thus 5 thermodynamical constants are required for each phase: $\gamma_k > 1$, $C_{V\,k} > 0$, $p_k^{\infty} > 0$, q_k and q_k'. We also need $(p_k + p_k^{\infty}) > 0$ in order to guarantee the positivity of some thermodynamical quantities. Finally, we use the estimations of the relaxation time scales τ_φ $(\varphi = p, \mu, u, T)$ provided in the previous section (equations (15)-(17)-(24)-(26)) with $\alpha_{min} = 0.2$ and $\alpha_{max} = 0.8$. All the following computations have been performed with the fast transient dynamics software Europlexus [2].

3.1 Canon experiment

The Canon experiment was carried out by Riegel [35] and studied the fast depressurization of hot liquid water (220°C and 32 bar). Figure 1 presents the experimental set-up, consisting in a 4.389 m long horizontal pipe, with an inner diameter of 102.3 mm. Pressure is measured at different locations along the pipe (from P1 to P5). The void fraction is also measured at location Pt (between P2 and P3 on figure 1) using a neutron scattering method.

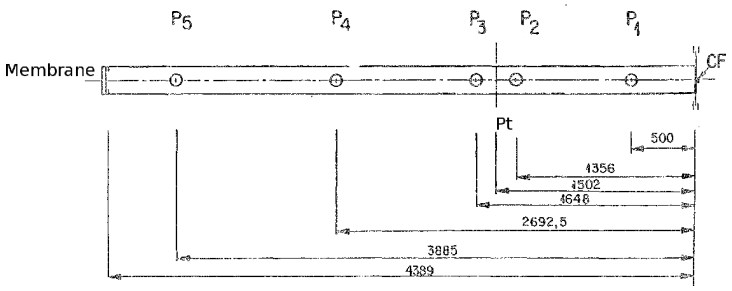

Figure 1: Schematic of Canon test facility

The parameters of the Stiffened Gas EOS for both phases are chosen to recover the steam-water phase diagram as in [9] and recalled in table 2. The computational domain is a 1D grid with a closed end at one side, and a tank, where atmospheric conditions are applied, on the other side. The initial conditions for the pipe and the tank are provided in table 3. Before comparing the experimental data and the numerical results obtained with the Bilicki-like mass transfer, we study the influence of the mesh refinements on the numerical results. Four different 1D grids with 10^3 to 10^4 cells are used in this study. The history of the void fraction at Pt obtained with those different grids is provided in figure 2. The gap between the results obtained with the coarsest grid and the results obtained with the finest one appears to be small. Refining the mesh only slightly delays the vaporisation process. We notice that grid independance is obtained from 5000 cells therefore the results obtained on this grid will be considered as converged results.

Table 2: EOS parameters for Canon experiment

	γ_k	p_k^∞ (Pa)	q_k (J.kg^{-1})	$C_{V\,k}$ (J.kg^{-1}.K^{-1})	q'_k (J.kg^{-1}.K^{-1})
vapor	1.34	0.00	2032350.00	1162.00	2351.11
liquid	1.66	769317123.86	-1359570.00	2807.61	11671.61

Table 3: Initial conditions for Canon experiment

		α_k	ρ_k (kg.m^{-3})	p_k (bar)	u_k (m.s^{-1})
Pipe	**vapor**	10^{-3}	16.72	32	0.00
	liquid	$1-10^{-3}$	841.12	32	0.00
Tank	**vapor**	$1-10^{-3}$	0.52	1	.
	liquid	10^{-3}	837.74	1	.

The comparison between the converged numerical results and the experimental data on the void fraction at Pt is shown on figure 3. We also add a reference numerical result without the Bilicki-like mass transfer obtained on the same grid with constant time scales, $\tau_\mu = 5\times10^{-5}$ s and $\tau_T = 10^{-7}$ s, as in a previous work [29]. An overall good agreement between the numerical and experimental results can be observed, with a complete vaporisation of the water. Although this vaporisation process happens earlier for both computations, the use of the Bilicki-like mass transfer delays it, which significantly improves the numerical results when compared with the experimental ones. Figure 4 provides the comparison between the measured pressure at P1 and the mean pressure $p = \alpha_v p_v + \alpha_l p_l$ obtained with the different computations. The experimental results show a sudden drop from the initial pressure 32 bar to 21 bar. Then the pressure remains constant at a saturation plateau until 400 ms and finally

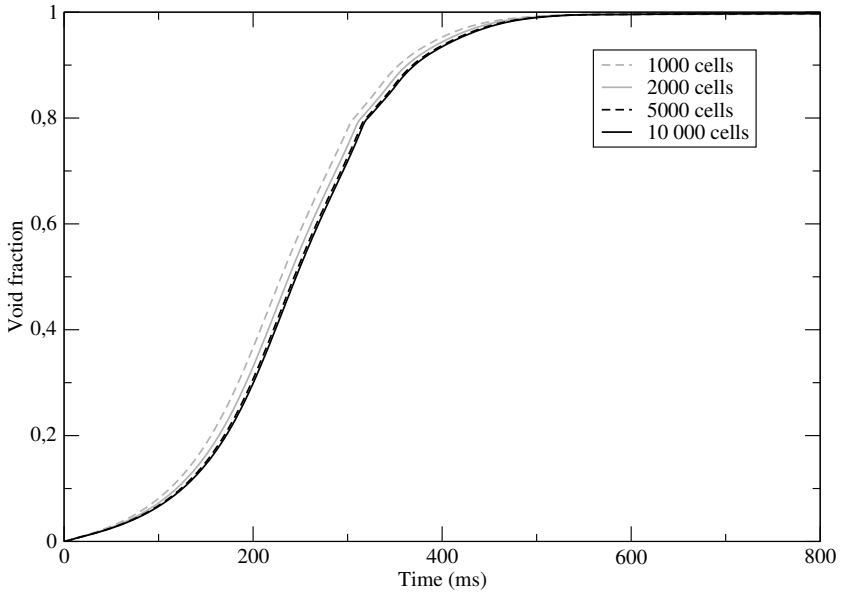

Figure 2: Influence of the grid refinement on the history of the void fraction at Pt in Canon experiment

slowly decreases towards the atmospheric pressure. The reference computation that uses constant time scales shows a plateau at 23 bar, the exact saturation pressure of the initial temperature, due to the fact that time scales remain very small. When compared with the experiment, this plateau appears to be slightly too high and too short. The results obtained with the Bilicki-like mass transfer show an important pressure undershoot before a pressure plateau at 20 bar. Unlike the reference computation, this plateau is slightly below the experimental one. We also notice that it is longer thanks to the proposed mass transfer, although the vaporisation process is predicted earlier in both computations. Apart from the undershoot before the plateau, the overall behavior of the pressure given by the two-fluid model with the Bilicki-like mass transfer is really similar to the measured pressure. We underline the fact that it delays the vaporisation and no longer imposes the saturation pressure when compared to the reference computation. Thus the Bilicki-like mass transfer appears to bring a significant improvement on the modelling of the vaporisation process with the two-fluid model ; nonetheless it needs to be assessed on other experimental cases.

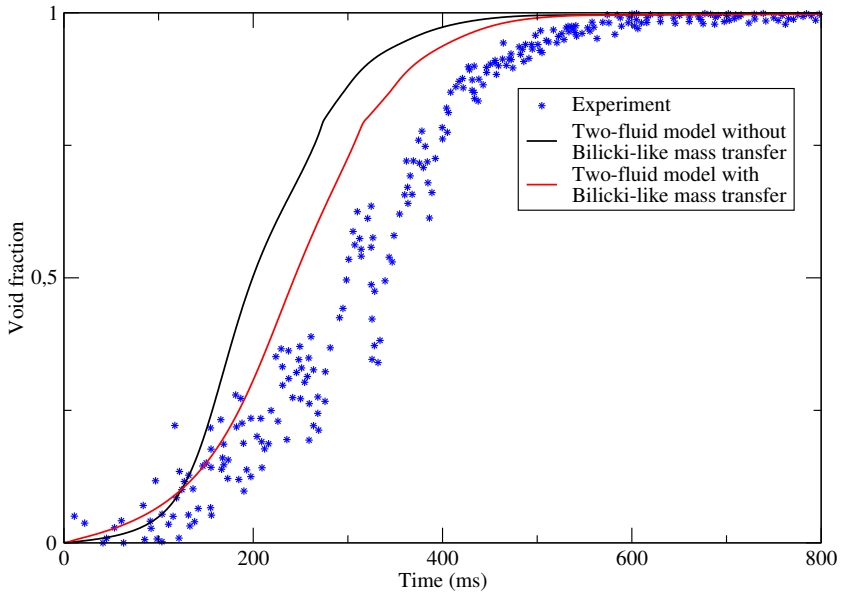

Figure 3: Void fraction vs time at Pt in Canon experiment: comparison between the experimental data, converged numerical results obtained with and without Bilicki-like mass transfer

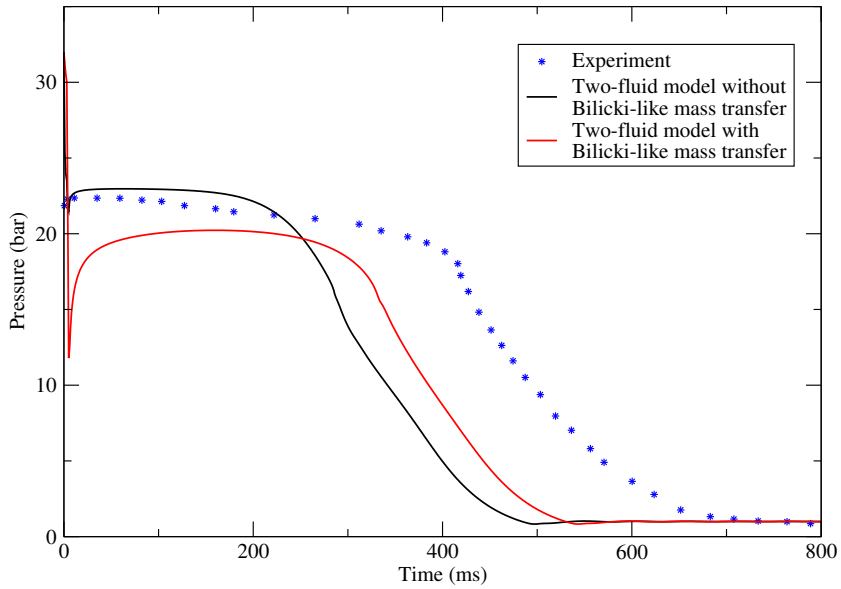

Figure 4: Pressure vs time at P1 in Canon experiment: comparison between the experimental data, converged numerical results obtained with and without Bilicki-like mass transfer

3.2 Super-Canon experiment

The Super-Canon experiment was also carried out by Riegel [35] with the same set-up as the Canon experiment (figure 1). The main difference between the two experiments lies in the initial conditions of the liquid water in the pipe which are the standard conditions of the primary loop in Pressurized Water Reactors (PWR): 300°C and 150 bar. Based on the initial temperature, the EOS parameters, gathered in table 4, are determined as before to retrieve the steam-water diagram [9]. Table 5 provides the initial conditions used in the computations.

Table 4: EOS parameters for Super-Canon experiment

	γ_k	p_k^∞ (Pa)	q_k (J.kg^{-1})	$C_{V\,k}$ (J.kg^{-1}.K^{-1})	q'_k (J.kg^{-1}.K^{-1})
vapor	1.49	0.00	2288300.00	603.37	4829.37
liquid	1.38	570798395.20	−1530700.00	3612.17	−515.21

Table 5: Initial conditions for Super-Canon experiment

		α_k	ρ_k (kg.m^{-3})	p_k (bar)	u_k (m.s^{-1})
Pipe	**vapor**	10^{-3}	88.23	150	0.00
	liquid	$1-10^{-3}$	736.45	150	0.00
Tank	**vapor**	$1-10^{-3}$	0.59	1	.
	liquid	10^{-3}	717.72	1	.

As in the previous case, a convergence study is carried out and suggests that numerical results obtained on the 5000-cell grid can be considered as converged results. Thus, we compare those numerical results obtained with the Bilicki-like mass transfer to the experimental results and to the results of a reference computation that uses constant time scales ($\tau_\mu = 5 \times 10^{-5}$ s and $\tau_T = 10^{-7}$ s). Figure 5 shows the comparison between those three results on the history of the void fraction at location Pt. If we first focus on the experimental data, we notice that the vaporisation process is similar to the one observed in the Canon experiment, despite the fact that it appears to be faster. We also observe that the measurements are more scattered in this case, particularly before 100 ms. Later on, it is easier to compare the experimental data with the numerical results. As it occurs in the Canon experiment, both computations show an earlier vaporisation but Bilicki-like mass transfer significantly reduces the gap between the computed results and the experimental ones. Then we compare the measured pressure at location P1 to the mean pressure $p = \alpha_v p_v + \alpha_l p_l$ from the computations (figure 6). The overall behavior of the pressure in the Super-Canon experiment is the same as in the Canon experiment: a sudden drop of pressure from the initial pressure to a plateau and a final slow decrease towards the external pressure. It is important to notice that the pressure level of the plateau, *i.e.* 60 bar, is very different from the saturation pressure of the initial temperature 86 bar unlike in the Canon experiment. Thus, the metastable states of water must be taken into account in the modelling process in order to retrieve the experimental data. When comparing the results of the reference computation to the experimental ones, we observe that the plateau of the computation is higher, around 80 bar, and really shorter. It shows that the use of small constant time scales is not relevant to capture metastable states since the pressure plateau is too close to the saturation pressure of the initial temperature. On the contrary, the computation with the Bilicki-like mass transfer provides a plateau with the same pressure level as in the experiment. The main differences between those two results are the important numerical pressure undershoot before the plateau and a shorter plateau obtained by the computation. Apart from those differences, the overall behavior of the pressure history obtained with the Bilicki-like mass transfer is really close to the experimental history. Thus it confirms the modelling choice of the mass transfer, especially regarding metastable states of water.

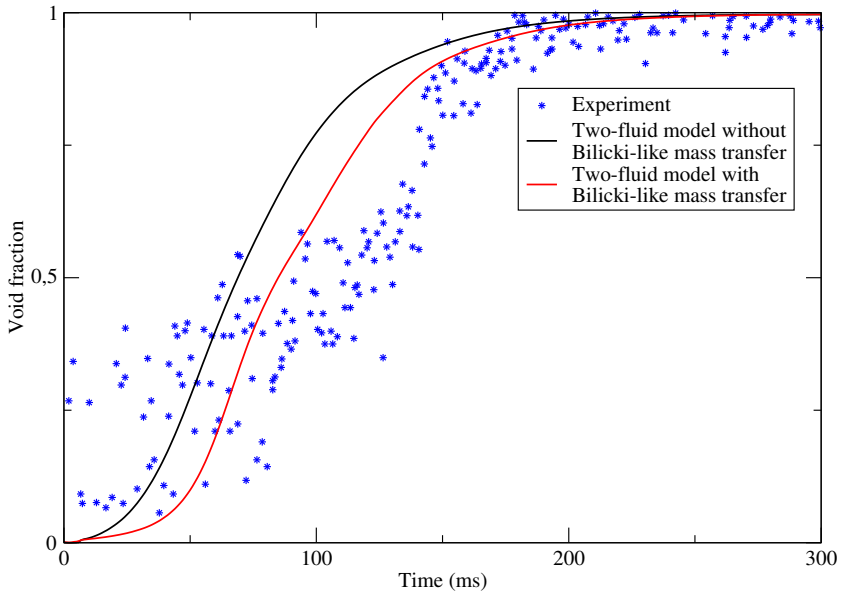

Figure 5: Void fraction vs time at Pt in Super-Canon experiment: comparison between the experimental data, converged numerical results obtained with and without Bilicki-like mass transfer

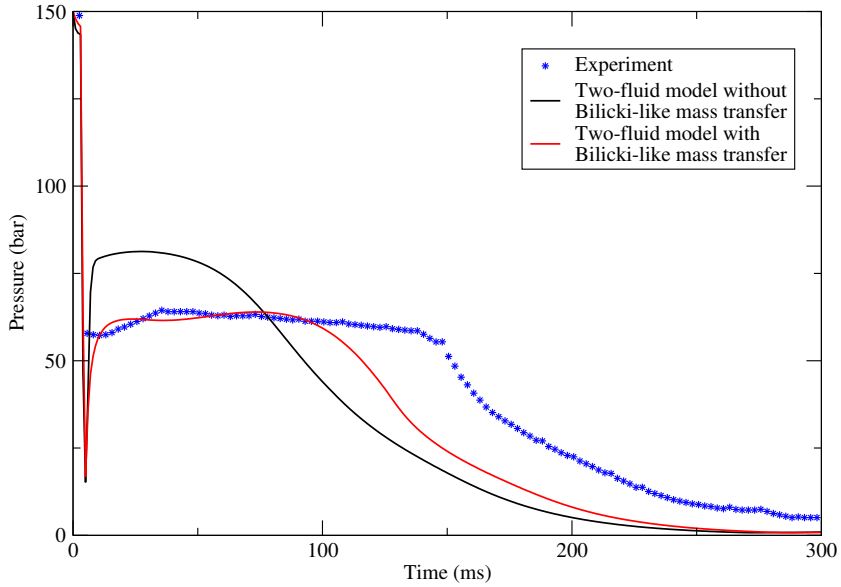

Figure 6: Pressure vs time at P1 in Super-Canon experiment: comparison between the experimental data, converged numerical results obtained with and without Bilicki-like mass transfer

3.3 Edwards pipe experiment

We study a third experiment of rapid depressurization of water carried out by Edwards and O'Brien [12]. The horizontal pipe used in the experiment is 4.097 m long and its inner diamater is 7.315 cm. One end of the pipe is closed and the other end has a membrane which is broken at the initial time. Unlike the previous experiments, the cross section of the break is 12.5% smaller than the cross section of the pipe. Different sensors are located around the pipe as shown in figure 7. Pressure is measured at both ends of the pipe ($GS1$ and $GS7$) and temperature is measured at $GS5$. A X-ray densitometer is also located at $GS5$ to measure the void fraction.

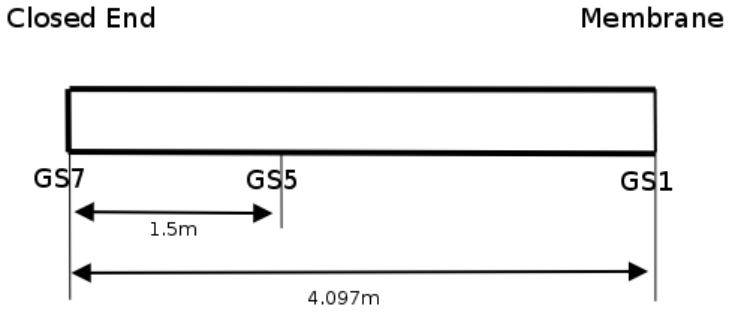

Figure 7: Schematic of the Edwards pipe

The initial conditions for the water in the pipe are 241.85°C and 70 bar. Since the initial temperature is close to the one of Canon experiment, we use the same EOS parameters recalled in table 6. The initial conditions for the computations are provided in table 7. For simplicity, we consider a full break and use 1D grids. As previously, different mesh refinements are used showing that the results on the 5000-cell grid can be considered as mesh independent.

Table 6: EOS parameters for Edwards pipe experiment

	γ_k	p_k^∞ (Pa)	q_k (J.kg^{-1})	$C_{V\,k}$ (J.kg^{-1}.K^{-1})	q'_k (J.kg^{-1}.K^{-1})
vapor	1.34	0.00	2032350.00	1162.00	2351.11
liquid	1.66	769317123.86	−1359570.00	2807.61	11671.61

Table 7: Initial conditions for Edwards pipe experiment

		α_k	ρ_k (kg.m^{-3})	p_k (bar)	u_k (m.s^{-1})
Pipe	**vapor**	10^{-3}	35.03	70	0.00
	liquid	$1-10^{-3}$	809.40	70	0.00
Tank	**vapor**	$1-10^{-3}$	0.50	1	.
	liquid	10^{-3}	802.20	1	.

Figure 8 provides the comparison of the experimental and numerical results on the void fraction. We first notice that only a few void fraction measurements are available in this experiment unlike the previous ones. Thus we only compare the overall behavior of the void fraction and we draw the same conclusion as for the Super-Canon experiment. Indeed, we observe that both numerical results have the same behavior, although the Bilicki-like mass transfer delays the vaporisation process which drives the results really close to the experimental data. At the same location, the temperature is also measured

in the experiment so we can also compare it to the numerical results. Figure 9 provides the comparison between those measurements and the mean temperature $T = \frac{m_v C_{V\,v} T_v + m_l C_{V\,l} T_l}{m_v C_{V\,v} + m_l C_{V\,l}}$, corresponding to the total internal energy, obtained in the computations. We can see that all curves first show a plateau between 500 K and the initial temperature 515 K. This plateau appears to be really short for the reference computation and longer when Bilicki-like mass transfer is used, though not as long as the experimental one. Then we observe a rapid decrease for both computations and the temperature finally remains steady around 380 K whereas a slower regular decrease is observed on the experimental results until the final time. This faster decrease of the temperature on the computational results is linked to a faster vaporisation. Moreover, the final constant temperature observed on the numerical results is due to the fact that no heat diffusion is taken into account in the numerical model. Finally, we compare the experimental pressure history at GS7 with the numerical mean pressure $p = \alpha_v p_v + \alpha_l p_l$ (figure 10). This comparison appears to be really similar as the comparison of the pressure history on Super-Canon experiment. On the one hand, the reference computation with constant time scales provides a short pressure plateau at 34 bar, really close to the saturation pressure 34.5 bar at the initial temperature. On the other hand, the experimental results show a longer plateau at 27 bar and the use of Bilicki-like mass transfer leads to a pressure plateau at 28 bar. As observed on the void fraction history, it also delays the vaporisation and we obtain a longer pressure plateau, which is closer to the experimental one. Thus the proposed modelling of the mass transfer provides a significant improvement of the numerical results obtained with the Baer-Nunziato model when compared with the experimental results. Some differences are still observed, particularly a slightly earlier vaporisation and a pressure undershoot in the first milliseconds of the computation.

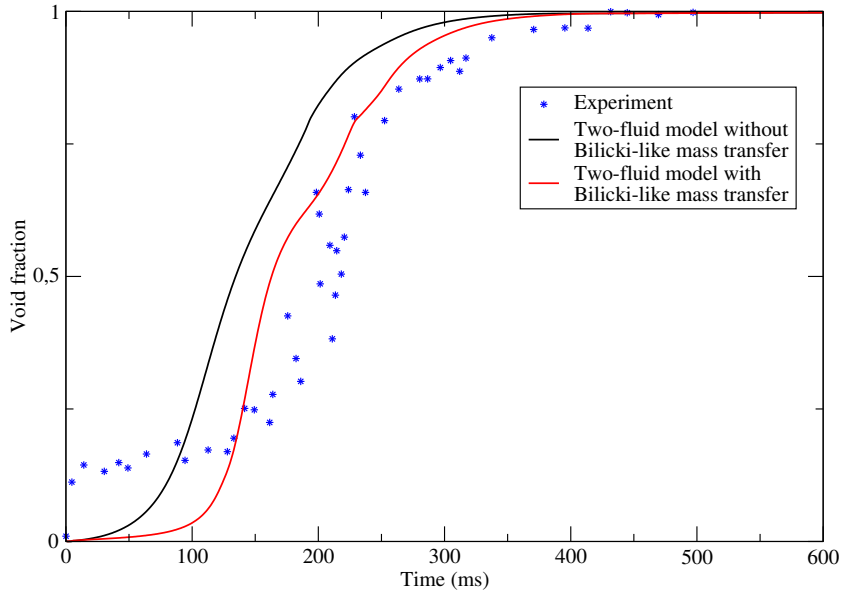

Figure 8: Void fraction vs time at GS5 in Edwards pipe experiment: comparison between the experimental data, converged numerical results obtained with and without Bilicki-like mass transfer

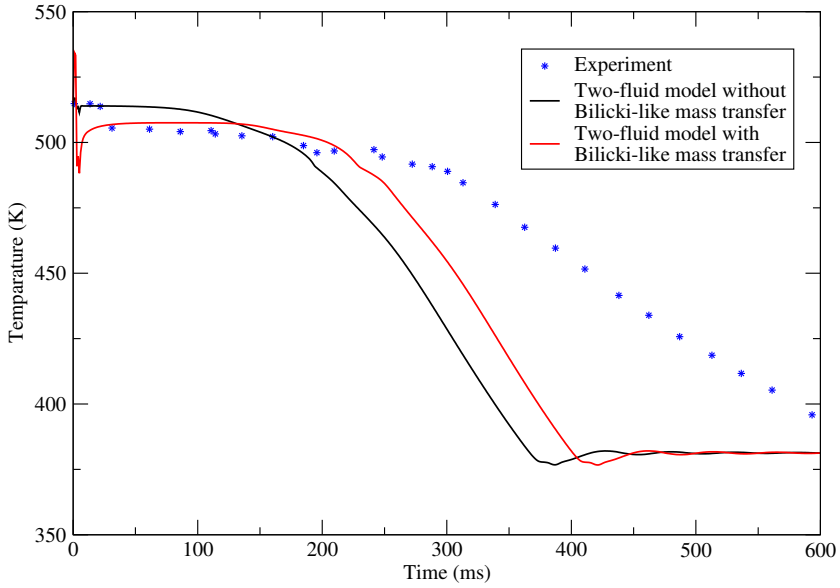

Figure 9: Temperature vs time at GS5 in Edwards pipe experiment: comparison between the experimental data, converged numerical results obtained with and without Bilicki-like mass transfer

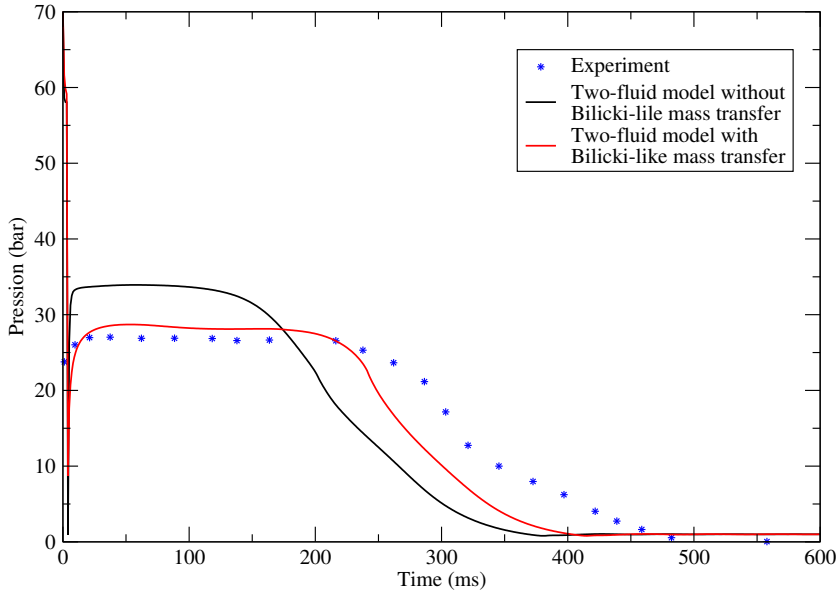

Figure 10: Pressure vs time at GS7 in Edwards pipe experiment: comparison between the experimental data, converged numerical results obtained with and without Bilicki-like mass transfer

3.4 HDR experiment

The last test-case considered here is the HDR (Heißdampfreaktor) experiment [37] which studies the LOCA on a full-scale reactor vessel unlike the previous test-cases. The experimental setup is presented in figure 11. It consists of a rigid pressure vessel with a single discharge nozzle and a simplified representation of the internals, including a flexible core barrel firmly clamped at its upper flange and a massive ring attached to the core barrel bottom to simulate the core mass. Different tests have been carried out on this vessel and we select the test V32 since it involves the most severe depressurization. In this case, the initial pressure in the vessel is 110 bar and the initial temperature varies from 221.6°C in the lower plenum to 308°C in the upper one. A membrane at the end of the nozzle is broken at the initial time, generating a rarefaction wave propagating along the pipe toward the vessel. Pressures in the vessel and core barrel displacements are measured at different locations. Thus the mechanical consequences of the depressurization can be studied in order to assess the two-fluid model.

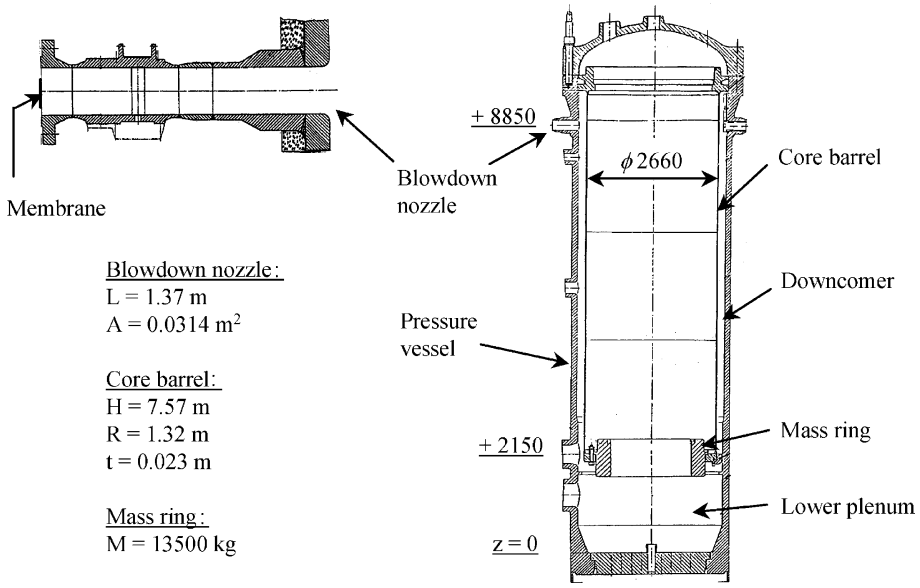

Figure 11: Schematic of the HDR pressure vessel

Unlike previous test-cases, a 3D fluid-structure computation is required to simulate the HDR experiment. The fast transient dynamics software Europlexus [2] uses a classical Arbitrary Lagrangian-Eulerian (ALE) formulation in order to compute Fluid-Structure interactions. More details on the computation of the Baer-Nunziato model using ALE formulation can be found in [8]. Based on the symmetry, the computational domain consists in half of the vessel, as presented in figure 12. The fluid and the structure are meshed in a conforming way with 5.8×10^6 finite volumes for the fluid, 68×10^3 shells elements for the core barrel and 11×10^3 solid elements for the mass ring. The computation of the 80 ms of physical time lasts around 15 hours on 80 CPU, with a Courant number $C_{CFL} = 0.9$ based on the celerity of pressure waves in the structure. Since the initial temperature in the pipe, where the vaporization occurs, is close to the one in Canon experiment, we use the same EOS parameters recalled in table 8. The structures are considered as linear elastic materials whose characteristics are detailed in table 9. Finally, table 10 provides the initial conditions for the computation. The temperature gradient in the vessel is neglected and the initial conditions of the nozzle (110 bar and 240°C) are applied in the whole vessel. As in the previous test-cases, atmospheric conditions are used in the tank representing the exterior medium. Since the physical time of the experiment is very short (80 ms), mass transfer is only considered in the nozzle therefore only pressure and velocity relaxations are applied in the vessel.

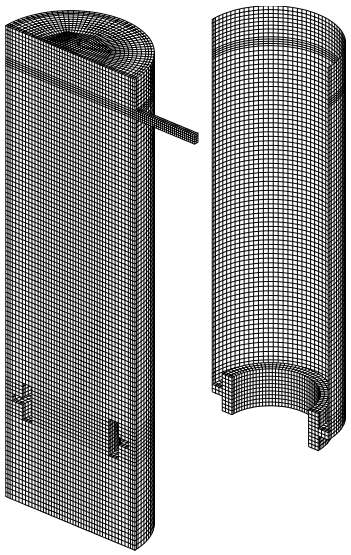

Figure 12: 3D mesh for the HDR experiment (Fluid mesh on the left and structure mesh on the right)

Table 8: EOS parameters for HDR experiment

	γ_k	p_k^∞ (Pa)	q_k (J.kg^{-1})	$C_{V\,k}$ (J.kg^{-1}.K^{-1})	q'_k (J.kg^{-1}.K^{-1})
vapor	1.34	0.00	2032350.00	1162.00	2351.11
liquid	1.66	769317123.86	−1359570.00	2807.61	11671.61

Table 9: Mechanical parameters for HDR experiment

	Density (kg.m^{-3})	**Young's modulus** (GPa)	**Poisson's ratio**
Mass ring	10612.2	175	0.295
Core barrel	7790	175	0.295

Table 10: Initial conditions for HDR experiment

		α_k	ρ_k (kg.m^{-3})	p_k (bar)	u_k (m.s^{-1})
Vessel and nozzle	**vapor**	10^{-6}	55.25	110	0.00
	liquid	$1-10^{-6}$	816.50	110	0.00
Tank	**vapor**	$1-10^{-6}$	0.52	1	.
	liquid	10^{-6}	837.74	1	.

Figure 13 provides the comparison between the experimental measurements and the numerical mean pressure histories $p = \alpha_v p_v + \alpha_l p_l$ at different locations in the vessel. For all the selected sensors, the results issuing from the experiment show a decrease of the pressure, from 110 bar to about 90 bar. The pressure decrease is really smooth for sensors far from the nozzle (see BP8302 on the bottom

right). For sensors closer to the nozzle, a greater pressure decrease is observed between 10 and 20 ms, then pressure remains constant around 100 bar, or even increases (see BP9136 on the top right), and finally decreases again after 55 ms. If we focus on the numerical results, similar trends are observed, however pressure decreases towards a lower value, slightly under 80 bar. Moreover, for sensors close to the nozzle, we notice that the mean pressure remains constant between 20 and 55 ms around 96 bar ; no increase of pressure is observed. When comparing experimental and numerical results, the main difference lies in the fact that pressure is underestimated in the numerical simulations due to a faster decrease. It results in a relative error of 10% at the end of the computation. This difference may be due to the fact that an instantaneous full break is considered in the numerical simulation resulting in a faster discharge of the vessel in the computation.

The histories of both pressure difference and displacement are provided in figure 14. A similar behavior of the pressure differences can be observed on the different experimental histories. Indeed, it first decreases to reach a minimum value at 25 ms due to the fact that the rarefaction wave is propagating in the downcomer before reaching the internal part of the core barrel. Then, pressure differences increase towards a maximum at 55 ms and finally decrease to reach a slightly negative value at the final time. The numerical results show a very good agreement with those experimental results on pressure difference histories. Similar maximum and minimum values can be observed and occur around the same time. This agreement shows that the behavior of the pressure wave is accurately captured in the computation, despite the underestimation of the absolute pressure mentionned earlier. Unlike pressure measurements, the behavior of the radial displacement of the core barrel really differs from one sensor to another. Due to the pressure difference between the internal part of the core barrel, we first observe that the radial displacement increases to reach a maximum value, then it decreases before increasing again. The value of the maximum, as well as the corresponding time, differs a lot depending on the location of the sensor. When compared with the experimental measurements, the numerical results show a rather good agreement. Some differences can be observed on the second half of the computation for KS1023 (at the top) and displacement is underestimated for KS1030 (in the middle) despite a similar behavior. On the whole, a good agreement is observed between numerical and experimental results during the first half of the computation for both pressure difference and displacement histories. More discrepancies appear during the second half and they may be linked to numerical diffusion since first order schemes are used in the computation. Thus, this last test-case shows that the proposed two-fluid model is also relevant for steam-water applications with Fluid-Structure Interactions and can be used on industrial-sized applications.

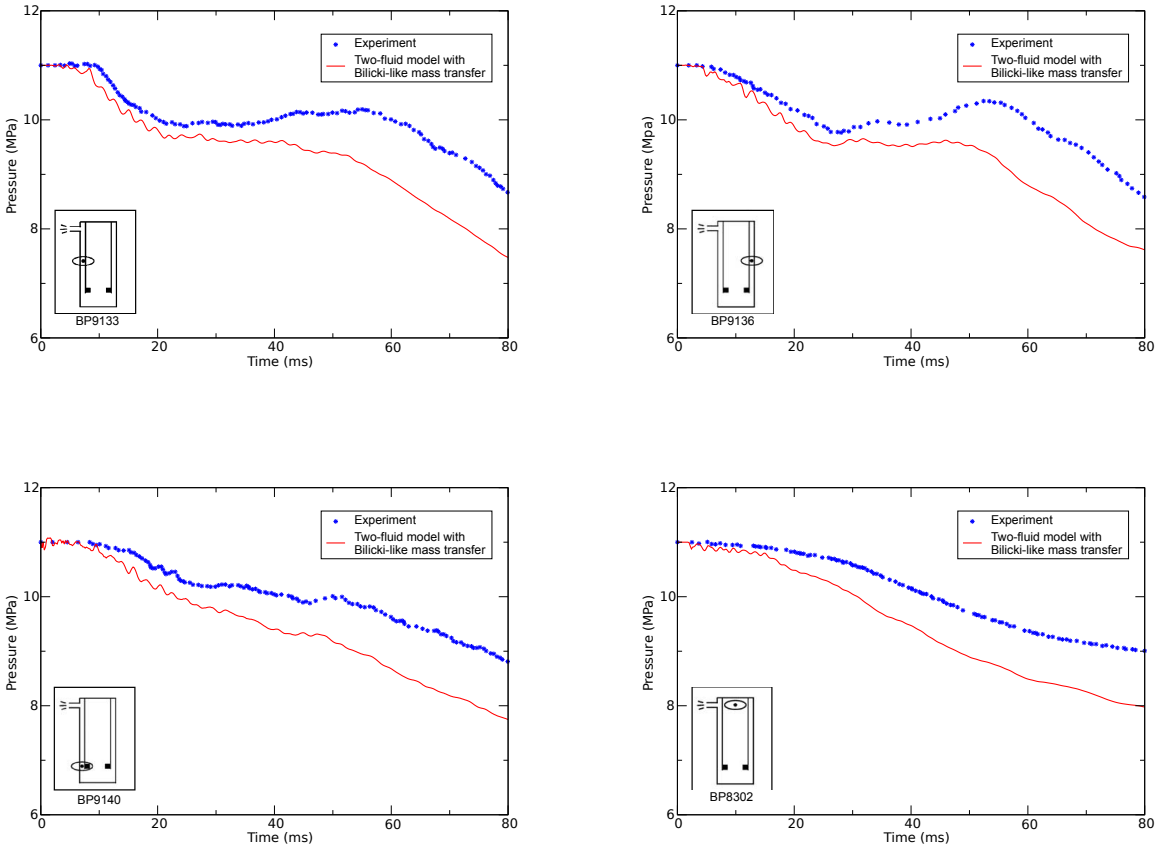

Figure 13: Pressure histories at different locations in the vessel

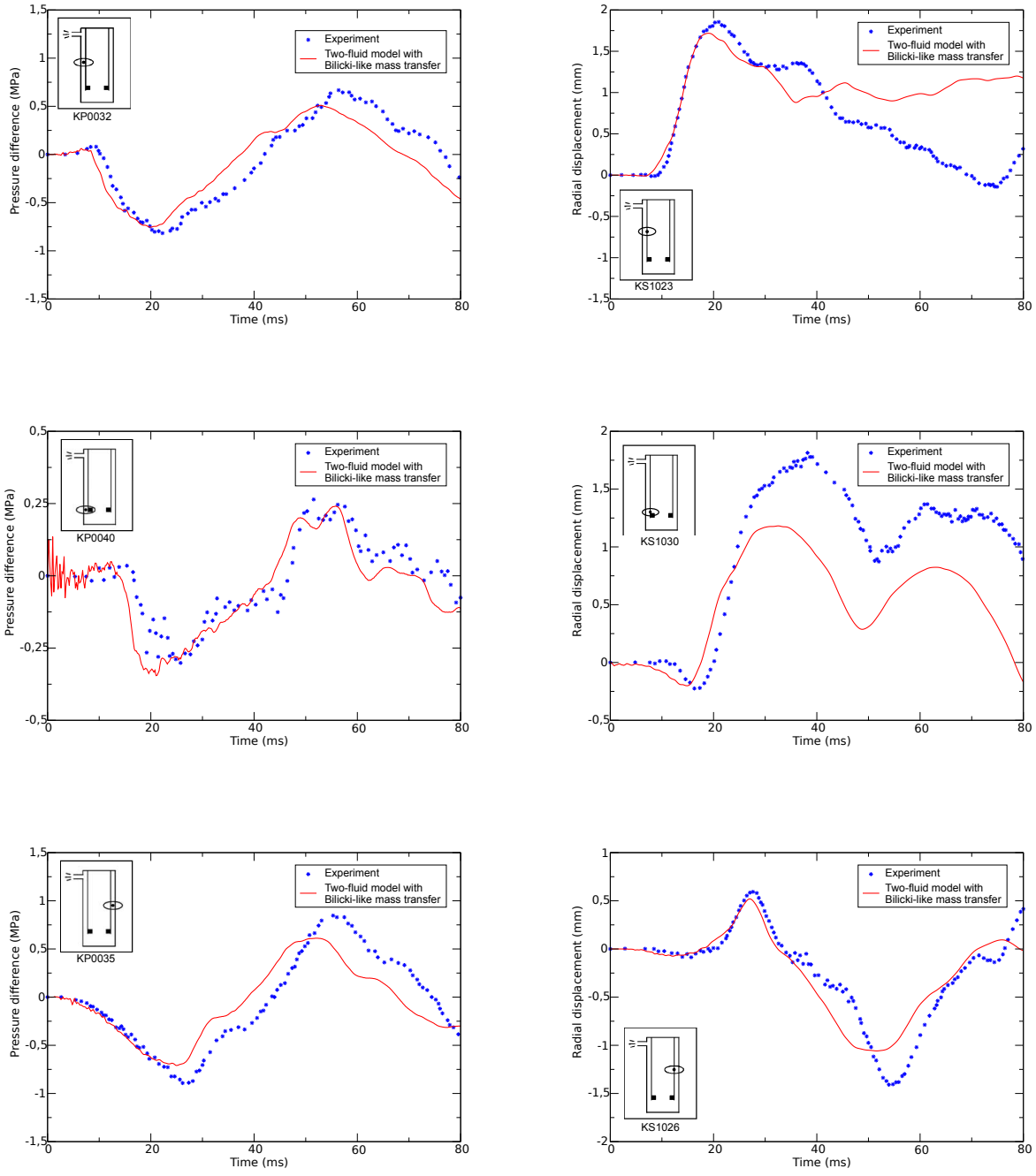

Figure 14: Pressure difference (on the left) and displacement (on the right) histories at different locations in the vessel

4 Conclusion

A two-fluid model has been used to compute fast depressurization of water. Based on the work of Baer & Nunziato [3], this two-fluid model does not assume any equilibrium between the phases. Thus the exchanges between phases must be taken into account and they are modelled as relaxation phenomena. Evaluations of the corresponding relaxation time scales must be provided. For pressure and velocity, previous work has been used [29], nevertheless the chemical potential relaxation, which corresponds to the mass transfer, requires particular attention. In order to model it in a simple but physically-relevant way, the work of Bilicki *et al.* [4, 10], based on the Homogeneous Relaxation Model, has been revisited. Thus, a new modelling of the mass transfer in the two-fluid frame is proposed. Four different experiments have been selected in order to assess the corresponding model. Three of them, the Canon, Super-Canon and Edwards pipe experiments, study the depressurization of a hot liquid water in a pipe. The comparisons between grid-converged computational results and experimental data show that the proposed Bilicki-like mass transfer significantly improves the results of the two-fluid model, particularly regarding pressure measurements. Moreover, it appears to be relevant for a wide range of thermodynamical states, including metastable states of water. The last test-case is the HDR experiment where pressures and displacements are measured in a full-scale vessel under the hypothesis of a Loss Of Coolant Accident. The results of an ALE computation show the ability of the proposed model to retrieve experimental data in both the structure and the fluid on an industrial-sized transient application.

The assessment of the proposed modelling of the mass transfer should be extended to other steam-water transients. Although the use of the Stiffened Gas Equation Of State appears to be quite relevant in the present work, the proposed modelling should also be tested with more realistic Equations Of State. To that end, the schemes dedicated to the treatment of the source terms should be extended and the convective solver proposed in previous work [30] could be used. Finally, extension of the current numerical methods to higher order should be considered in order to lower the computational cost of the two-fluid model on industrial applications.

Acknowledgements The first author received a financial support through the EDF-CIFRE contract 0459-2013. Computational facilities were provided by EDF and CEA. Numerical simulations have been performed with the *Europlexus* software.

The Homogeneous Relaxation Model

The Homogeneous Relaxation Model (HRM) proposed by Bilicki and Kestin [4] consists in the usual three conservation laws for the two-phase mixture and the mass conservation law for one of the phases. Thus ρ denotes the mean density of the two-phase mixture, u its mean velocity, p its mean pressure and e its mean specific total energy. We also denote α_k the mean volume fraction of phase k and ρ_k its mean density, complying with:

$$\left\{ \begin{array}{l} \alpha_v + \alpha_l = 1 \\ m_v + m_l = \rho \\ m_k = \alpha_k \rho_k \end{array} \right. \tag{28}$$

The specific total energy of the mixture is given by the following relation:

$$e = \varepsilon + \frac{1}{2} u^2 \tag{29}$$

where an Equation Of State for the two-phase mixture is required:

$$\varepsilon = \varepsilon \left(\alpha_k, \rho, p \right) \tag{30}$$

Thanks to the different notations, the governing equations of the HRM model are the following:

$$\left\{ \begin{array}{lcll} \partial_t \left(\alpha_k \rho_k \right) & + & \partial_x \left(\alpha_k \rho_k u \right) & = & \Gamma_k^{HRM} \\ \partial_t \left(\rho \right) & + & \partial_x \left(\rho u \right) & = & 0 \\ \partial_t \left(\rho u \right) & + & \partial_x \left(\rho u^2 + p \right) & = & 0 \\ \partial_t \left(\rho e \right) & + & \partial_x \left(\rho e u + p u \right) & = & 0 \end{array} \right. \tag{31}$$

Bilicki and Kestin [4] propose a simple form of closure law for the mass transfer:

$$\Gamma_k^{HRM} = - \frac{m_k - \overline{m_k}}{\theta} \tag{32}$$

where the notation $\overline{\varphi}$ stands for the quantity φ at the thermodynamical and chemical equilibrium. This simple relaxation equation gives its name to the model and requires a relaxation time scale θ.

References

[1] RELAP5-3D Code Manual Volume IV: Models and Correlations. Technical Report INEEL-EXT-98-00834, Idaho National Laboratory (INL), 2012.
URL `http://www4vip.inl.gov/relap5/r5manuals/ver_4_0/vol-4.pdf`

[2] Europlexus User's Manual. Technical Report, Joint Research Centre (JRC), Commissariat à l'énergie atomique et aux énergies alternatives (CEA), 2016.
URL `http://europlexus.jrc.ec.europa.eu/public/manual_html/index.html`

[3] M. Baer and J. Nunziato. A two-phase mixture theory for the deflagration-to-detonation transition (DDT) in reactive granular materials. *International Journal of Multiphase Flow*, 12(6):861–889, 1986.

[4] Z. Bilicki and J. Kestin. Physical aspects of the relaxation model in two-phase flow. *Proceedings of the Royal Society of London A: Mathematical, Physical and Engineering Sciences*, 428(1875):379–397, 1990.

[5] Z. Bilicki, R. Kwidziński, and S. A. Mohammadein. Evaluation of the relaxation time of heat and mass exchange in the liquid-vapour bubble flow. *International Journal of Heat and Mass Transfer*, 39(4):753–759, 1996.

[6] F. Coquel, T. Gallouët, J.-M. Hérard, and N. Seguin. Closure laws for a two-fluid two-pressure model. *Comptes Rendus Mathematique*, 334(10):927–932, 2002.

[7] F. Crouzet, F. Daude, P. Galon, J.-M. Hérard, O. Hurisse, and Y. Liu. Validation of a two-fluid model on unsteady liquid-vapor water flows. *Computers & Fluids*, 119:131–142, 2015.

[8] F. Daude and P. Galon. On the computation of the Baer-Nunziato model using ALE formulation with HLL- and HLLC-type solvers towards fluid-structure interactions. *Journal of Computational Physics*, 304:189–230, 2016.

[9] F. Daude, P. Galon, Z. Gao, and E. Blaud. Numerical experiments using a HLLC-type scheme with ALE formulation for compressible two-phase flows five-equation models with phase transition. *Computers & Fluids*, 94:112–138, 2014.

[10] P. Downar-Zapolski, Z. Bilicki, L. Bolle, and J. Franco. The non-equilibrium relaxation model for one-dimensional flashing liquid flow. *International Journal of Multiphase Flow*, 22(3):473–483, 1996.

[11] D. A. Drew and S. L. Passman. *Theory of Multicomponent Fluids*. Springer Verlag, 1999.

[12] A. R. Edwards and T. P. O'Brien. Studies of phenomena connected with the depressurization of water reactors. *Journal of the British Nuclear Energy Society*, 9:125–135, 1970.

[13] P. Embid and M. Baer. Mathematical analysis of a two-phase continuum mixture theory. *Continuum Mechanics and Thermodynamics*, 4(4):279–312, 1992.

[14] E. Faucher, J.-M. Hérard, M. Barret, and C. Toulemonde. Computation of flashing flows in variable cross-section ducts. *International Journal of Computational Fluid Dynamics*, 13(4):365–391, 2000.

[15] J. Gale, I. Tiselj, and A. Horvat. Two-fluid model of the WAHA code for simulations of water hammer transients. *Multiphase Science and Technology*, 20(3-4):291–322, 2008.

[16] T. Gallouët, J.-M. Hérard, and N. Seguin. Numerical Modeling Of Two-Phase Flows Using The Two-Fluid Two-Pressure Approach. *Mathematical Models and Methods in Applied Sciences*, 14(05):663–700, 2004.

[17] S. Gavrilyuk. The structure of pressure relaxation terms : one-velocity case. Internal report H-I83-2014-00276-EN, EDF R&D, 2014.

[18] S. Gavrilyuk and R. Saurel. Mathematical and Numerical Modeling of Two-Phase Compressible Flows with Micro-Inertia. *Journal of Computational Physics*, 175(1):326–360, 2002.

[19] J. Glimm, D. Saltz, and D. H. Sharp. Renormalization group solution of two-phase flow equations for Rayleigh-Taylor mixing. *Physics Letters A*, 222(3):171–176, 1996.

[20] J. Glimm, D. Saltz, and D. H. Sharp. Two-phase modelling of a fluid mixing layer. *Journal of Fluid Mechanics*, 378:119–143, 1999.

[21] V. Guillemaud. *Modélisation et simulation numérique des écoulements diphasiques par une approche bifluide à deux pressions*. Ph.D. thesis, Université de Provence - Aix-Marseille I, 2007. URL `https://tel.archives-ouvertes.fr/tel-00169178/document`

[22] J.-M. Hérard and O. Hurisse. A fractional step method to compute a class of compressible gas-liquid flows. *Computers & Fluids*, 55:57–69, 2012.

[23] M. Ishii. *Thermo-fluid dynamic theory of two-phase flows*. Collection de la Direction des Etudes et Recherches d'Electricité de France, 1975.

[24] H. Jin, J. Glimm, and D. H. Sharp. Entropy of averaging for compressible two-pressure two-phase flow models. *Physics Letters A*, 360(1):114–121, 2006.

[25] A. K. Kapila, S. F. Son, J. B. Bdzil, R. Menikoff, and D. S. Stewart. Two-phase modeling of DDT: Structure of the velocity-relaxation zone. *Physics of Fluids*, 9(12):3885–3897, 1997.

[26] J. Lavieville, M. Boucker, E. Quemerais, S. Mimouni, and N. Mechitoua. NEPTUNE_CFD V1.0 - Theory Manual. Internal report H-I81-2006-04377-EN, EDF R&D, 2006.

[27] O. Le Métayer, J. Massoni, and R. Saurel. Dynamic relaxation processes in compressible multiphase flows. Application to evaporation phenomena. *ESAIM: Proceedings*, 40:103–123, 2013.

[28] H. Lochon. *Modélisation et simulation d'écoulements transitoires eau-vapeur en approche bifluide*. Ph.D. thesis, Université d'Aix-Marseille, 2016.

[29] H. Lochon, F. Daude, P. Galon, and J.-M. Hérard. Comparison of two-fluid models on steam-water transients. *ESAIM: Mathematical Modelling and Numerical Analysis*, 2016.

[30] H. Lochon, F. Daude, P. Galon, and J.-M. Hérard. HLLC-type riemann solver with approximated two-phase contact for the computation of the baer–nunziato two-fluid model. *Journal of Computational Physics*, 326:733–762, 2016.

[31] S. Müller, M. Hantke, and P. Richter. Closure conditions for non-equilibrium multi-component models. *Continuum Mechanics and Thermodynamics*, pages 1–33, 2015.

[32] M. Pelanti and K.-M. Shyue. A mixture-energy-consistent six-equation two-phase numerical model for fluids with interfaces, cavitation and evaporation waves. *Journal of Computational Physics*, 259:331–357, 2014.

[33] V. H. Ransom and D. L. Hicks. Hyperbolic two-pressure models for two-phase flow. *Journal of Computational Physics*, 53(1):124–151, 1984.

[34] M. Reocreux. *Contribution à l'étude des débits critiques en écoulement diphasique eau-vapeur*. Ph.D. thesis, Université Scientifique et Médicale de Grenoble, 1974.

[35] B. Riegel. *Contribution à l'étude de la décompression d'une capacité en régime diphasique*. Ph.D. thesis, Université Scientifique et Médicale et Institut National Polytechnique de Grenoble, 1978.

[36] R. Saurel and R. Abgrall. A Multiphase Godunov Method for Compressible Multifluid and Multiphase Flows. *Journal of Computational Physics*, 150(2):425–467, 1999.

[37] L. Wolf. Experimental results of coupled fluid-structure interactions during blowdown of the HDR-vessel and comparisons with pre-and post-test predictions. *Nuclear Engineering and Design*, 70(3):269–308, 1982.